



Application of anodic oxidation, electro-Fenton and UVA photoelectro-Fenton to decolorize and mineralize acidic solutions of Reactive Yellow 160 azo dye



Alejandro Bedolla-Guzman^a, Ignasi Sirés^{b,1}, Abdoulaye Thiam^b,
Juan Manuel Peralta-Hernández^{1,a,**}, Silvia Gutiérrez-Granados^{a,1}, Enric Brillas^{1,b,*}

^a Departamento de Química, División de Ciencias Naturales y Exactas, Universidad de Guanajuato, Cerro de la Venada s/n, Pueblito de Rocha, Guanajuato, Mexico

^b Laboratori d'Electroquímica dels Materials i del Medi Ambient, Departament de Química Física, Facultat de Química, Universitat de Barcelona, Martí i Franquès 1-11, 08028 Barcelona, Spain

ARTICLE INFO

Article history:

Received 4 February 2016

Received in revised form 27 April 2016

Accepted 27 April 2016

Available online 28 April 2016

Keywords:

Anodic oxidation
Electro-Fenton
Photoelectro-Fenton
Reactive Yellow 160
Water treatment

ABSTRACT

The degradation of 100 cm³ of a solution with 0.167 mmol dm⁻³ Reactive Yellow 160 (RY160) azo dye in sulfate medium at pH 3.0 has been comparatively studied by anodic oxidation with electrogenerated H₂O₂ (AO-H₂O₂), electro-Fenton (EF) and UVA photoelectro-Fenton (PEF). Trials were carried out with a stirred tank reactor equipped with a boron-doped diamond (BDD) anode and an air-diffusion cathode for H₂O₂ production, upon addition of 0.50 mmol dm⁻³ Fe²⁺ as catalyst in EF and PEF. The solution was slowly decolorized by AO-H₂O₂ because of the low rate of reaction of the azo dye and its colored products with hydroxyl radicals generated at the BDD anode from water oxidation. The color loss was enhanced in EF by the larger oxidation ability of hydroxyl radicals produced in the bulk from Fenton's reaction between added Fe²⁺ and generated H₂O₂, whereas the solution was more rapidly decolorized by PEF owing to the additional generation of hydroxyl radicals from the photolysis of Fe(III)-hydroxy complexes by UVA light. The relative mineralization ability of the processes also increased in the sequence AO-H₂O₂ < EF < PEF. The PEF method was the most powerful due to the synergistic oxidation by hydroxyl radicals and UVA irradiation, yielding 94% mineralization after 360 min at 100 mA cm⁻². The influence of current density and RY160 concentration on the performance of all processes was assessed. Final carboxylic acids like maleic, fumaric, tartronic, acetic, oxalic, oxamic and formic were quantified by ion-exclusion HPLC. All these acids were totally removed by PEF, but the formation of small amounts of other highly recalcitrant products impeded the total mineralization. Chloride, sulfate, ammonium and, to a smaller extent, nitrate ions were released to the solution from the heteroatoms of the azo dye in all cases.

© 2016 Elsevier Ltd. All rights reserved.

1. Introduction

The manufacture of leather products, along with the availability of raw materials and labor, has favored the development of the tanning industry. Currently, Mexico is among the ten world's largest producers of pelts, accounting for 4% of total production.

The Guanajuato region is the largest National producer, generating about 65% of tanning and leather finishing. In the city of Leon, for example, there are more than 500 tanneries, thus constituting its main economic activity. Leather production is divided into four stages: riviera, tanning, RTE (retanning, dyeing, greasing) and finishing. At the end, the leather has acquired softness, and especially color, among other features that are necessary to produce commercial products. Dyeing is a chemical process that imparts color to the leather in the drum. Coloring can be just superficial or reach the entire thickness of leather and, for this purpose, direct and basic anionic dyes are used to avoid adding trills. In this context, the wastewater treatment containing

* Corresponding author. Tel.: +34 934021223; fax: +34 934021231.

** Corresponding author.

E-mail addresses: juan.peralta@ugto.mx (J.M. Peralta-Hernández), brillas@ub.edu (E. Brillas).

¹ ISE Active Member.

industrial dyes, produced as a result of the increasing activity of the tannery industry in Guanajuato state, is a coordinated task between the society and government, aiming to avoid their noxious effects on the aquatic environment, animals and human beings [1].

For the remediation of dyeing wastewater, different traditional physicochemical techniques including adsorption, coagulation and filtration have been tested [2–4]. Although these methods can yield fast decolorization, they generate large volumes of sludge to be disposed and/or need the regular regeneration of adsorbent materials. Recently, advanced oxidation processes (AOPs) have appeared as powerful alternatives for the treatment of such wastewater since they are able to transform the organic pollutants into innocuous substances [5–8]. AOPs are based on the in situ generation of very oxidizing reactive oxygen species (ROS) such as the free hydroxyl radical ($\cdot\text{OH}$). When it is generated, $\cdot\text{OH}$ can react quickly and non-selectively with most organics, being added to a double bond or abstracting a hydrogen atom, reaching their mineralization in many cases, i.e., their conversion into CO_2 and H_2O .

Lately, the electrochemical advanced oxidation processes (EAOPs) based on Fenton's reaction chemistry have received increasing attention for the treatment of acidic wastewater [9–12]. The significance of these methods is due to their environmental compatibility, amenability of automation, high energy efficiency, versatility and safe operation under mild conditions. In these EAOPs, hydrogen peroxide is electrochemically supplied to the treated solution by the two-electron reduction of O_2 gas, preferentially at a carbonaceous cathode as follows [9,11]:



Carbon nanotubes [13,14], activated carbon fiber [15,16], carbon sponge [17], graphite [18], graphite felt [19], carbon felt [19–23], carbon-polytetrafluoroethylene (PTFE) gas (O_2 or air) diffusion [24–27] and boron-doped diamond (BDD) [28–30] have been used to electrogenerate H_2O_2 from reaction (1). Since H_2O_2 is a weak oxidant, its oxidation power is greatly improved by the addition of Fe^{2+} to the acidic solution to form $\cdot\text{OH}$ and Fe^{3+} according to Fenton's reaction (2), with optimum pH of 2.8 [9,11,12,31,32]:



This EAOP is commonly referred to as electro-Fenton (EF), whose main advantage compared to chemical Fenton's reagent is the propagation of reaction (2) from the reduction of Fe^{3+} to Fe^{2+} at the cathode through reaction (3) [9,12]:

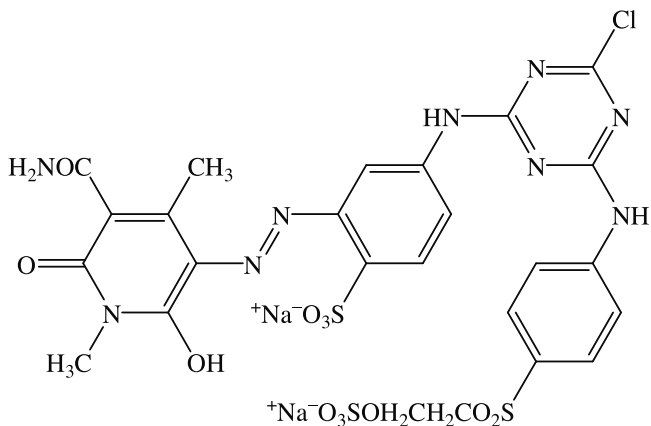


Fig. 1. Chemical structure of Reactive Yellow 160.

The principal reason for combining on-site H_2O_2 generation and Fenton's reaction (2) is the enhancement of the oxidation abilities of the two individual treatments, creating a synergistic EF system. When this process is performed in an undivided cell with a large O_2 -overpotential anode M, organics are destroyed by both, $\cdot\text{OH}$ formed in the bulk from Fenton's reaction (2) and physisorbed hydroxyl radicals originated at the anode surface from water oxidation ($\text{M}(\cdot\text{OH})$) [9,12,32,33]. Wastewater decontamination based on the removal of pollutants upon the sole action of the anode (without Fenton's reagent) gives rise to the well-known and popular anodic oxidation (AO) method, whereas if H_2O_2 is produced at the cathode, it is so-called AO with electrogenerated H_2O_2 (AO- H_2O_2) [11,32]. Currently, BDD thin-layer electrodes are considered the best anodes for AO and AO- H_2O_2 since they can efficiently mineralize a large number of aromatics and aliphatic carboxylic acids [34–37]. The generation of the physisorbed oxidant BDD($\cdot\text{OH}$) at the BDD anode proceeds as follows:



An important limitation of the EF treatment of azo dyes is the production of final Fe(III) -carboxylate complexes that are very hardly attacked by generated hydroxyl radicals [38–42]. This drawback can be solved by illuminating the solution with UVA radiation supplied by a lamp in the so-called UVA photoelectro-Fenton (PEF) process [9,11,39–42], which favors: (i) the enhancement of Fe^{2+} regeneration and $\cdot\text{OH}$ production by photoreduction of Fe(OH)^{2+} , the predominant Fe(III) species at pH ~ 3.0 , from reaction (5) and (ii) the photodecarboxylation of Fe(III) -

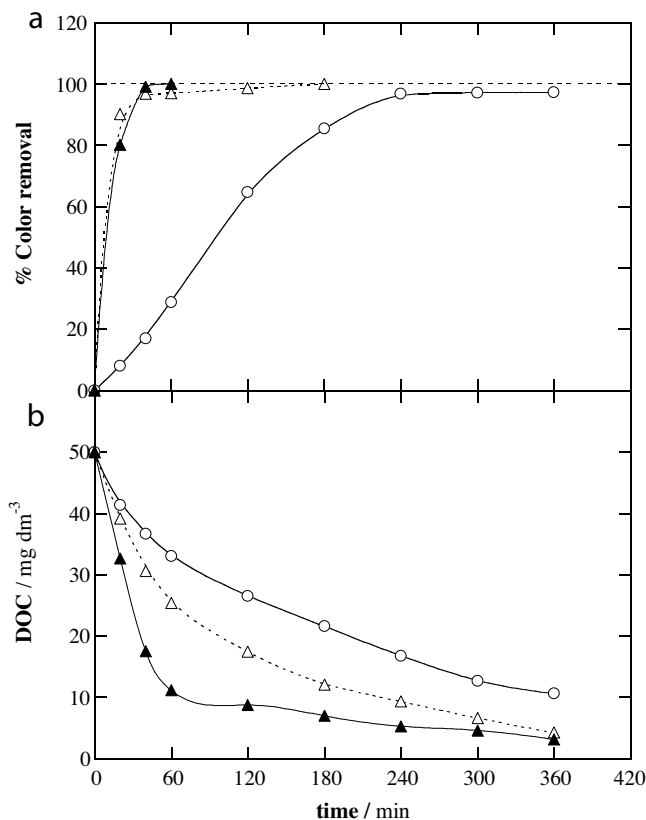
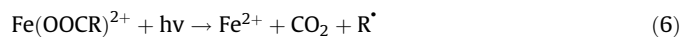


Fig. 2. (a) Decolorization efficiency and (b) dissolved organic carbon (DOC) removal with electrolysis time for the treatment of 100 cm^3 of a solution of $0.167 \text{ mmol dm}^{-3}$ RY160 with $0.050 \text{ mol dm}^{-3}$ Na_2SO_4 at pH 3.0 using a stirred tank reactor equipped with a 3 cm^2 BDD anode and a 3 cm^2 air-diffusion cathode at 100 mA cm^{-2} and 25°C . (○) Anodic oxidation with electrogenerated H_2O_2 (AO- H_2O_2), (△) electro-Fenton (EF) with $0.50 \text{ mmol dm}^{-3}$ Fe^{2+} and (▲) photoelectro-Fenton (PEF) with $0.50 \text{ mmol dm}^{-3}$ Fe^{2+} and a 6 W UVA light.

carboxylate intermediates from the general reaction (6) [43]:



To gain a better understanding on the viability of EAOPs to decolorize and mineralize azo dyes, we have undertaken a study on the degradation of a complex azo dye, Reactive Yellow 160 (RY160, $\text{Na}_2\text{C}_{25}\text{H}_{22}\text{ClN}_9\text{O}_{12}\text{S}_3$, $M = 818.13 \text{ g mol}^{-1}$, $\lambda_{\text{max}} = 440 \text{ nm}$, see formula in Fig. 1), widely used in many tannery factories in the Guanajato region. Only one paper dealing with the AO of this azo dye using

different PbO_2 -based and SnO_2 -based anodes has been previously reported in the literature [44].

This paper presents the results obtained for the comparative color removal and mineralization of RY160 solutions by applying AO- H_2O_2 , EF and PEF with a BDD anode and a carbon-PTFE air-diffusion cathode. The effect of the applied current density (j) and azo dye content on the degradation by each EAOP was examined to better clarify the role of generated hydroxyl radicals and/or UVA irradiation. Final short-linear aliphatic carboxylic acids and released inorganic ions were quantified by high-performance liquid chromatography (HPLC) and ion chromatography, respectively.

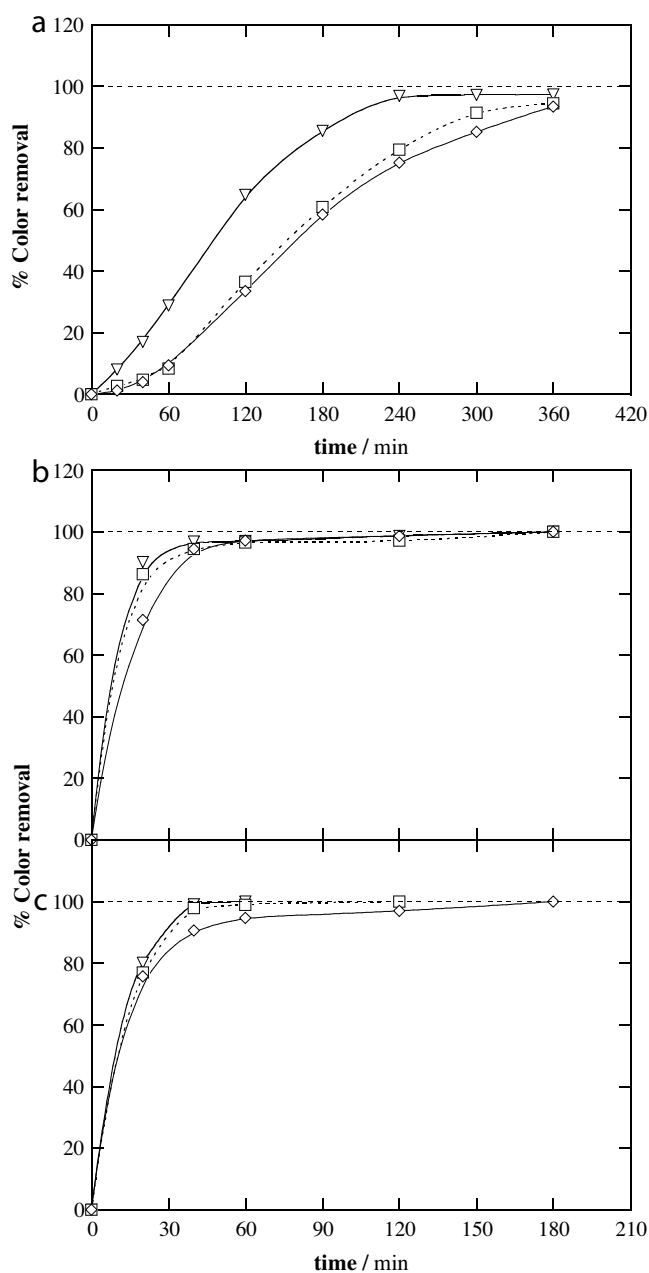


Fig. 3. Effect of current density on the percentage of color removal vs electrolysis time for the degradation of 100 cm^3 of a $0.167 \text{ mmol dm}^{-3}$ RY160 and $0.050 \text{ mol dm}^{-3}$ Na_2SO_4 solution at pH 3.0 and 25°C using a stirred BDD/air-diffusion cell. (a) AO- H_2O_2 , (b) EF and (c) PEF. Applied current density: (\diamond) 33.3 mA cm^{-2} , (\square) 66.7 mA cm^{-2} and (∇) 100 mA cm^{-2} .

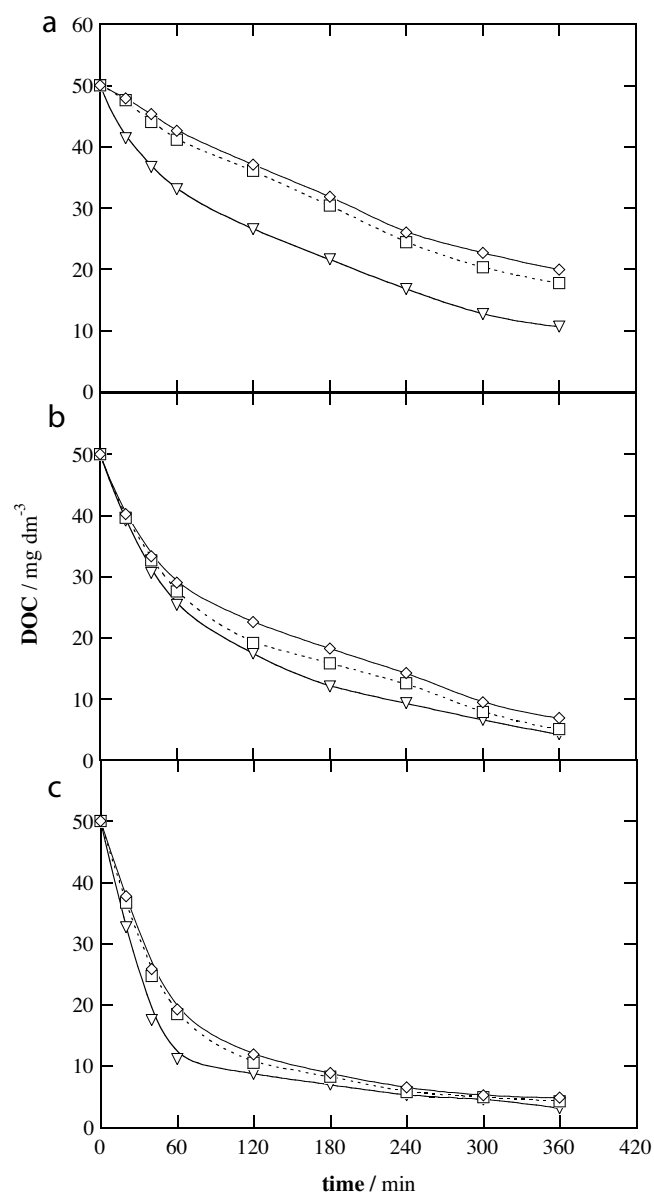


Fig. 4. Change of DOC with electrolysis time for the assays of Fig. 3. (a) AO- H_2O_2 , (b) EF and (c) PEF. Applied current density: (\diamond) 33.3 mA cm^{-2} , (\square) 66.7 mA cm^{-2} and (∇) 100 mA cm^{-2} .

2. Experimental

2.1. Chemicals

Commercial RY160 (66% content, plus inorganic salts for stabilization) was supplied by PCL S.A. de C.V (Mexico). The solutions were prepared with ultrapure water from a Millipore Milli-Q system (resistivity > 18 M Ω cm, 25 °C). The catalyst and background electrolyte were introduced as FeSO₄·7H₂O and anhydrous Na₂SO₄, both of analytical grade purchased from Fluka and Panreac, respectively. The solution pH was adjusted to 3.0 with analytical grade H₂SO₄ supplied by Merck. Carboxylic acids, solvents and other chemicals were either of analytical or HPLC grade purchased from Panreac and Sigma-Aldrich.

2.2. Electrochemical system

The electrolytic experiments were performed in batch mode at laboratory scale using an open, cylindrical and undivided two-electrode cell containing a 100 cm³ RY160 solution. The cell was surrounded by a jacket where thermostated water was recirculated to keep the solution at 25 °C. In all trials, the solution was vigorously stirred with a magnetic bar at 800 rpm for the mixing of organics and their mass transport toward/from the electrodes. The anode was a 3 cm² BDD thin film purchased from NeoCoat and the cathode was a carbon-PTFE air-diffusion electrode supplied by E-TEK. The inter-electrode gap was about 1 cm. The cathode was mounted as described elsewhere [45] and was fed with pumped air at a flow rate of 1 dm³ min⁻¹ for H₂O₂ generation by reaction (1). All the trials were made at constant j provided by an EG&G PAR 273A potentiostat-galvanostat. For the PEF runs, the solution was illuminated with a 6W Philips black light blue tube lamp of

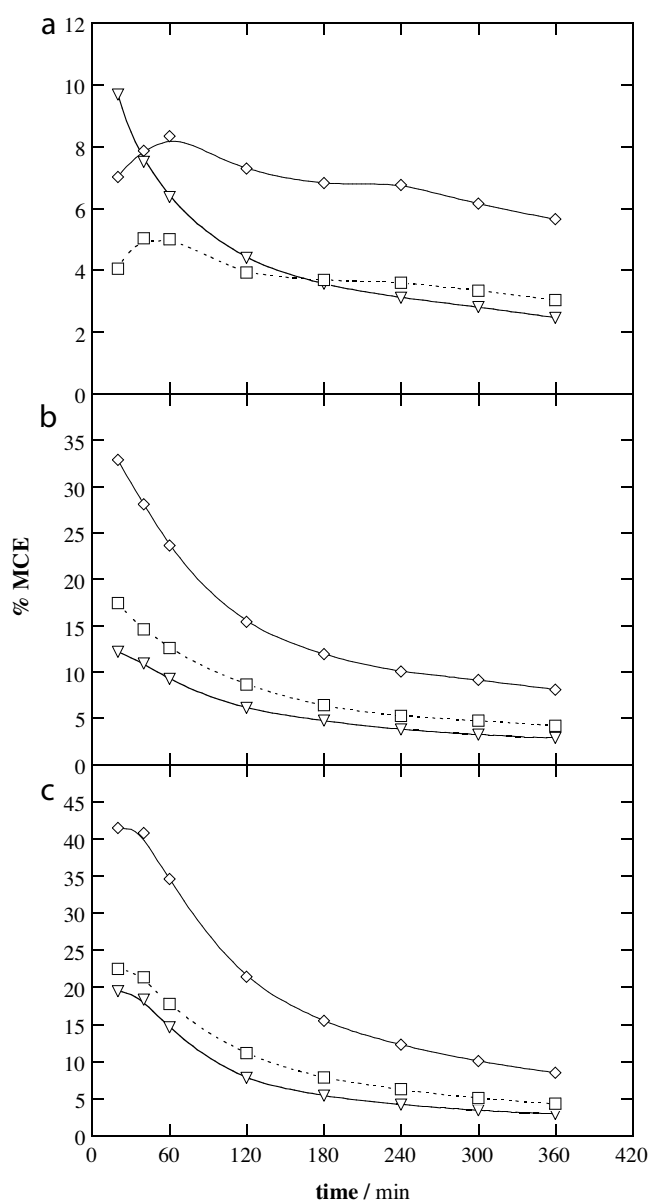


Fig. 5. Mineralization current efficiency calculated from Eq. (10) vs electrolysis time for the trials of Fig. 3 and 4. (a) AO-H₂O₂, (b) EF and (c) PEF. Applied current density: (\diamond) 33.3 mA cm⁻², (\square) 66.7 mA cm⁻² and (∇) 100 mA cm⁻².

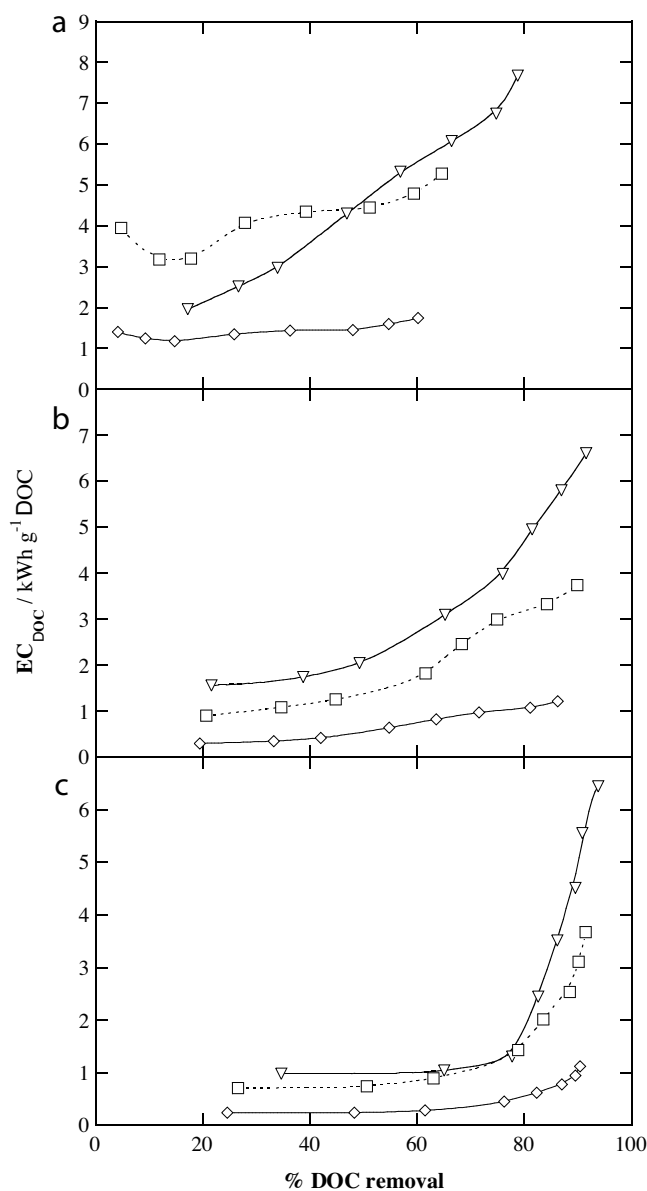


Fig. 6. Variation of the specific energy consumption per unit DOC mass obtained from Eq. (11) with percentage of DOC removal for the experiments shown in Fig. 3 and 4. (a) AO-H₂O₂, (b) EF and (c) PEF. Applied current density: (\diamond) 33.3 mA cm⁻², (\square) 66.7 mA cm⁻² and (∇) 100 mA cm⁻².

$\lambda_{\max} = 360$ nm, placed 7 cm above it and supplying an UV irradiance of 5 W m^{-2} , as detected with a Kipp & Zonen CUV 5 global UV radiometer. Cleaning of the BDD surface and activation of the air-diffusion cathode were made before the treatments by polarizing 100 cm^3 of $0.050 \text{ mol dm}^{-3} \text{ Na}_2\text{SO}_4$ at 100 mA cm^{-2} for 180 min.

Solutions with 0.167 and $0.333 \text{ mmol dm}^{-3}$ of RY160, equivalent to 50 and 100 mg dm^{-3} of dissolved organic carbon (DOC), respectively, in $0.050 \text{ mol dm}^{-3} \text{ Na}_2\text{SO}_4$ were degraded at pH 3.0 by means of AO- H_2O_2 , EF and PEF. The influence of j between 33.3 and 100 mA cm^{-2} on the performance of each EAOP was assessed. In all the EF and PEF assays, $0.50 \text{ mmol dm}^{-3} \text{ Fe}^{2+}$ was initially added to the solution to act as catalyst of Fenton's reaction (2).

2.3. Instruments and analytical procedures

The solution pH was determined with a Crison GLP 22 pH-meter. Samples withdrawn from electrolyzed solutions were microfiltered with $0.45 \mu\text{m}$ PTFE filters from Whatman prior to immediate analysis. Hydrogen peroxide concentration was measured from the light absorption of the titanous-hydrogen peroxide complex at $\lambda = 408$ nm using a Shimadzu Unicam 1800 UV-vis spectrophotometer thermostated at 25°C [46]. The loss of solution color was followed from their absorbance (A) decay at the maximum visible wavelength of $\lambda_{\max} = 440$ nm of RY160, determined with the above spectrophotometer. The decolorization efficiency or percentage of color removal was determined by measuring the change from the starting absorbance A_0 to the value A_t at time t , as follows [11,12]:

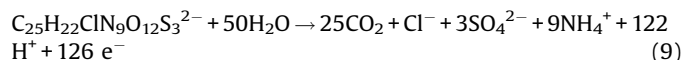
$$\% \text{Color removal} = \frac{A_0 - A_t}{A_0} \times 100 \quad (7)$$

The mineralization of electrolyzed solutions was assessed from their DOC decay, measured on a Shimadzu VCSN TOC analyzer. This analysis was made by injecting $50 \mu\text{L}$ aliquots into this system, obtaining reproducible DOC values with $\pm 1\%$ accuracy. The percentage of DOC removal for a given experiment at time t was then calculated from Eq. (8) [12]:

$$\% \text{DOC removal} = \frac{\Delta(\text{DOC})_{\text{exp}}}{\text{DOC}_0} \times 100 \quad (8)$$

where $\Delta(\text{DOC})_{\text{exp}}$ is the experimental DOC decay (in mg C dm^{-3}) and DOC_0 is the starting DOC.

The theoretical total mineralization of the anionic form of RY160 can be assumed to yield carbon dioxide and chloride, sulfate and ammonium as pre-eminent ions, as discussed below:



Then, the mineralization current efficiency (MCE, in %) for each trial was estimated as [38]:

$$\% \text{MCE} = \frac{nFV\Delta(\text{DOC})_{\text{exp}}}{4.32 \times 10^7 mlt} \times 100 \quad (10)$$

where $n = 126$ is the number of electrons for the total combustion of the azo according to reaction (9), F is the Faraday constant ($96,487 \text{ C mol}^{-1}$), V is the solution volume (in dm^3), 4.32×10^7 is a conversion factor ($3,600 \text{ s h}^{-1} \times 12,000 \text{ mg C mol}^{-1}$), $m = 25$ is the number of carbon atoms of RY160, I is the current (in A) and t is the electrolysis time (in h).

The specific energy consumption per unit DOC mass (EC_{DOC}) was estimated by Eq. (11) [12,38]:

$$\text{EC}_{\text{DOC}} (\text{kWh g}^{-1} \text{DOC}) = \frac{E_{\text{cell}} It}{V\Delta(\text{DOC})_{\text{exp}}} \quad (11)$$

where E_{cell} is the average cell voltage (in V) and the rest of parameters have been defined above. This equation is valid for AO- H_2O_2 and EF, but it is an approach for PEF because the energy required by the UVA lamp, which can be replaced by free sunlight [26], is not considered.

Short-linear aliphatic carboxylic acids were quantified by HPLC using a Waters 600 LC fitted with a Bio-Rad Aminex HPX 87H, $300 \text{ mm} \times 7.8 \text{ mm}$, column at 35°C , coupled to a Waters 996 photodiode array detector set at $\lambda = 210$ nm. In these analyses, aliquots of $20 \mu\text{L}$ were injected into the LC and a $4 \text{ mmol dm}^{-3} \text{ H}_2\text{SO}_4$ solution at $0.6 \text{ cm}^3 \text{ min}^{-1}$ was used as mobile phase. The chromatograms exhibited peaks at retention times of 7.0 min for oxalic acid, 7.9 min for tartronic acid, 8.2 min for maleic acid, 9.4 min for oxamic acid, 13.7 min for formic acid, 14.8 min for acetic acid and 15.7 min for fumaric acid. NH_4^+ , Cl^- , NO_3^- and SO_4^{2-} contents were analyzed by ion chromatography upon injection of $25 \mu\text{L}$ aliquots into a Shimadzu 10Avp LC coupled with a Shimadzu CDD 10Avp, following the procedure reported elsewhere [41].

3. Results and discussion

3.1. Characterization of the electrochemical systems

Prior to the degradation of RY160 solutions, the supporting electrolyte was treated under AO- H_2O_2 , EF and PEF conditions to clarify the ability of these EAOPs to produce and accumulate H_2O_2 . For each electrochemical system, 100 cm^3 of a $0.050 \text{ mol dm}^{-3} \text{ Na}_2\text{SO}_4$ solution at pH 3.0 and 25°C were electrolyzed at j values of 33.3 , 66.7 and 100 mA cm^{-2} for 360 min. Treatments under EF and

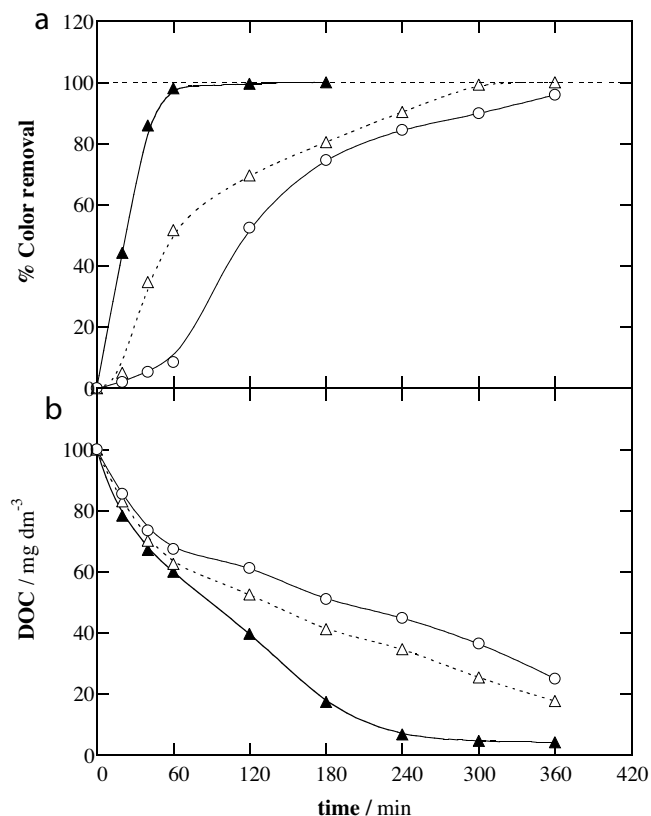


Fig. 7. (a) Percentage of color removal and (b) DOC vs electrolysis time for the: (○) AO- H_2O_2 , (△) EF and (▲) PEF treatments of 100 cm^3 of a solution of $0.334 \text{ mmol dm}^{-3}$ RY160 in $0.050 \text{ mol dm}^{-3} \text{ Na}_2\text{SO}_4$ at pH 3.0 using a stirred BDD/air-diffusion tank reactor at 100 mA cm^{-2} and 25°C . In EF and PEF, $0.50 \text{ mmol dm}^{-3} \text{ Fe}^{2+}$ was added to the initial solution.

PEF conditions were carried out with $0.50 \text{ mmol dm}^{-3} \text{ Fe}^{2+}$ as catalyst. No change of solution pH was found during these runs.

In all cases, the H_2O_2 content in solution rose rapidly at short electrolysis time, tending to a plateau at prolonged electrolysis time. The gradual decrease in the accumulation rate of H_2O_2 at long time can be related to the progressive increase in its decomposition rate as the oxidant concentration became higher. This phenomenon can be ascribed to the acceleration of H_2O_2 oxidation to O_2 at the BDD anode, with the weak oxidant hydroperoxyl radical (HO_2^\bullet) formed as intermediate as follows [11]:



The plateau in each trial is just attained when the rate for H_2O_2 generation from reaction (1) and its destruction from reactions (12) and (13) became equal. In AO- H_2O_2 , final concentrations of 33.4, 59.7 and $75.5 \text{ mmol dm}^{-3}$ were found for this species at 33.3, 66.7 and 100 mA cm^{-2} , respectively. The greater H_2O_2 accumulation at higher j can be explained by the concomitant upgrading of reaction (1), which also entails an acceleration of reactions (12) and (13). When the EF conditions were tested, the H_2O_2 content decayed up to 30.6, 45.8 and $57.8 \text{ mmol dm}^{-3}$ at the end of the electrolyses at the above j values, respectively. This decrease is due to the action of Fenton's reaction (2) promoting the removal of H_2O_2 content, to a larger extent when greater j was applied. The H_2O_2 concentration was even more sharply reduced under PEF conditions, attaining final values of 16.3, 23.8 and $28.1 \text{ mmol dm}^{-3}$ for the same j values, as a result of the production of more $^\bullet\text{OH}$ and quicker Fe^{2+} regeneration from photolytic reaction (5), which induces a greater acceleration of Fenton's reaction (2). These findings confirm the large ability of all the electrochemical systems to accumulate high amounts of H_2O_2 in the medium, which allow the production of enough $^\bullet\text{OH}$ in the bulk to effectively remove RY160 and its oxidation products.

An additional blank experiment was made by adding $0.167 \text{ mmol dm}^{-3}$ RY160 to the above supporting electrolyte and irradiating the resulting solution with a 6 W UVA lamp for 120 min without current supply. Neither decolorization nor DOC abatement were observed under these conditions, corroborating the high photostability of the azo dye upon UVA illumination and suggesting that its destruction in EAOPs can be basically caused by generated hydroxyl radicals.

3.2. Comparative decolorization and mineralization of RY160 solutions by EAOPs

A first series of comparative degradation assays was made by treating 100 cm^3 of a $0.167 \text{ mmol dm}^{-3}$ RY160 solution in $0.050 \text{ mol dm}^{-3} \text{ Na}_2\text{SO}_4$ at pH 3.0 and 25°C by AO- H_2O_2 , as well as by EF and PEF upon addition of $0.50 \text{ mmol dm}^{-3} \text{ Fe}^{2+}$, using a stirred BDD/air-diffusion cell at $j = 100 \text{ mA cm}^{-2}$ for 360 min. In these trials, the solution pH became slightly acid to reach a final value near 2.6–2.7, probably due to the production of acidic products like final carboxylic acids [38–42], as will be discussed below.

Fig. 2a depicts a very slow loss in solution color by applying AO- H_2O_2 , attaining 98% decolorization efficiency at the end of the treatment. This means that physisorbed BDD($^\bullet\text{OH}$) radicals originated from reaction (4) at the BDD anode attack very slowly the azo dye and its colored products, thus needing long time for removing the color. In contrast, Fig. 2a also highlights a very quick and complete decolorization in 180 min by EF, as a result of the additional oxidation of RY160 and colored products by $^\bullet\text{OH}$ formed in the bulk via Fenton's reaction (2). The decolorization process

was even much more rapid by using PEF, where the solution became colorless in only 60 min, as can be seen in Fig. 2a. This is due to the production of much larger quantities of $^\bullet\text{OH}$ in the bulk from the photolytic reaction (5), also yielding faster Fe^{2+} regeneration that enhances Fenton's reaction (2).

Products formed during the RY160 degradation were hardly transformed into CO_2 , as deduced from the larger time required for gradual mineralization compared with the time for total decolorization. Fig. 2b shows that the $0.167 \text{ mmol dm}^{-3}$ azo dye solution underwent a continuous DOC reduction with electrolysis time for all EAOPs, without attaining overall mineralization in any case. From these DOC-time plots, one can infer that the relative oxidation power increases in the sequence AO- $\text{H}_2\text{O}_2 < \text{EF} < \text{PEF}$, similarly to their decolorization ability. The slow degradation of organics by BDD($^\bullet\text{OH}$) at the BDD surface in AO- H_2O_2 only allowed attaining 79% DOC abatement in 360 min, whereas their additional oxidation by $^\bullet\text{OH}$ in the bulk upgraded the mineralization in EF reaching 91% DOC decay. PEF was the most powerful EAOP for both, decolorization and mineralization processes. In the latter case, Fig. 2b depicts a very quick DOC abatement up to 78% in only 60 min, owing to the large synergistic action of UVA light on initial photoactive by-products that favors their fast conversion into CO_2 . At longer time, however, DOC abatement rate was strongly reduced, attaining a final value of 94%. This suggests the formation of highly recalcitrant products at the end of PEF that are hardly removed by BDD($^\bullet\text{OH}$), $^\bullet\text{OH}$ and UVA radiation, thereby preventing the total mineralization of the azo dye solution.

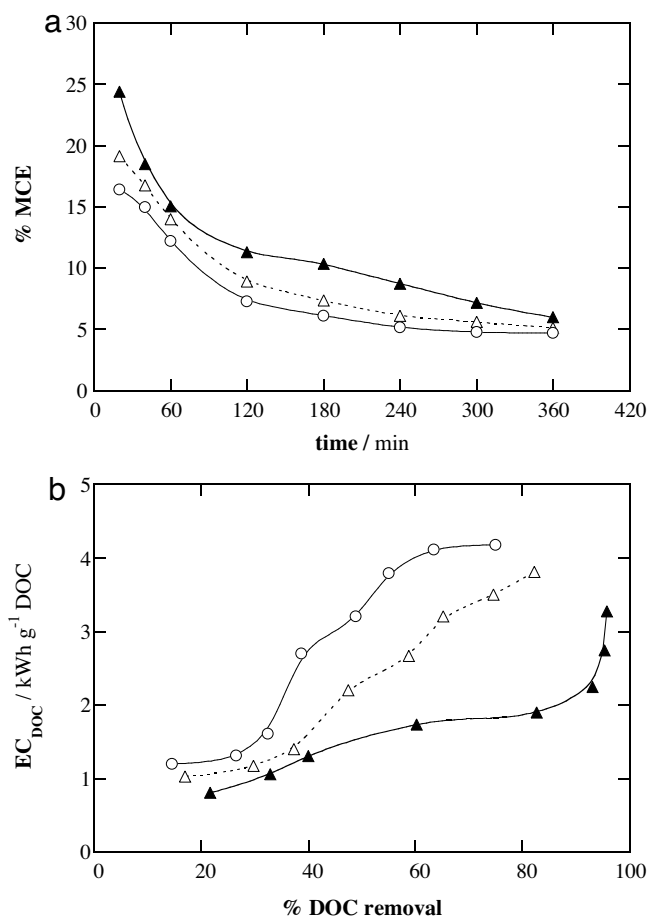


Fig. 8. Change of (a) mineralization current efficiency with electrolysis time and (b) specific energy consumption per unit DOC mass with percentage of DOC removal for the degradation trials of Fig. 7. (○) AO- H_2O_2 , (△) EF and (▲) PEF.

3.3. Effect of current density on the degradation of the azo dye solutions

The applied j is an important operation parameter in EAOPs because it determines the quantity of oxidizing hydroxyl radicals that are formed to destroy organic pollutants. The influence of this parameter on the degradation of a $0.167 \text{ mmol dm}^{-3}$ RY160 solution of pH 3.0 was then checked for the AO- H_2O_2 , EF and PEF processes between 33.3 and 100 mA cm^{-2} for 360 min. The solution pH in all these trials did not vary significantly and attained final values near 2.6–2.7 due to the formation of acidic products, as pointed out above.

The changes in decolorization efficiency with electrolysis time for the EAOPs at the three j values tested are presented in Fig. 3a–c. The percentage of color removal in each process always grew when j increased, at least at the beginning of the runs. This can be accounted for by the progressive production of larger amounts of BDD($\cdot\text{OH}$) from reaction (4) in all cases, as well as of $\cdot\text{OH}$ from Fenton's reaction (2) in EF and PEF because of the larger generation and accumulation of H_2O_2 in the bulk, as pointed out in section 3.1. For each j value, moreover, the decolorization efficiency decreased in the order $\text{PEF} > \text{EF} > \text{AO-}\text{H}_2\text{O}_2$, in agreement with their relative oxidation power. Fig. 3a shows that for the less potent process (AO- H_2O_2), higher j caused a larger loss of color until 240 min of electrolysis, whereupon it was decelerated up to attain quite similar decolorization efficiencies of 93%, 94% and 98% for 33.3, 66.7 and 100 mA cm^{-2} , respectively. This is indicative of the generation of very recalcitrant colored products that need long time to be removed by BDD($\cdot\text{OH}$). The production of great amounts of $\cdot\text{OH}$ with much higher oxidation ability to remove the azo dye and its colored products in EF gave rise to total decolorization in about 180 min for all j values, as can be observed in Fig. 3b. However, faster decolorization with increasing j from 33.3 to 100 mA cm^{-2} was found until 90 min, whereupon it was quite similar for all j values because of the slower removal of small amounts of very recalcitrant colored products. This phenomenon was less apparent in PEF as a result of the greater generation of $\cdot\text{OH}$ induced by photolytic reaction (5). For this treatment, Fig. 3c highlights that the azo dye solution became colorless after 180, 120 and 60 min of electrolysis at 33.3, 66.7 and 100 mA cm^{-2} , respectively. That means that the formation of oxidant $\cdot\text{OH}$ was significantly enhanced at higher j , which can be explained by the greater generation of H_2O_2 yielding larger quantities not only of $\cdot\text{OH}$ from Fenton's reaction (2), but also of Fe^{3+} that is more quickly photoreduced by reaction (5), eventually upgrading the Fe^{2+} regeneration and $\cdot\text{OH}$ formation.

An enhancement of DOC decay was always found when j rose from 33.3 to 100 mA cm^{-2} as a result of the greater generation of hydroxyl radicals, as stated above. Comparison of DOC- t plots of Fig. 4a–c corroborates again a decay in the relative oxidation power of EAOPs in the sequence $\text{PEF} > \text{EF} > \text{AO-}\text{H}_2\text{O}_2$, regardless of the applied j . For AO- H_2O_2 , Fig. 4a clearly shows that the oxidative action of increasing amounts of BDD($\cdot\text{OH}$) led to higher DOC reduction, reaching 60%, 65% and 79% at the end of the treatment at 33.3, 66.7 and 100 mA cm^{-2} , respectively. The additional production of $\cdot\text{OH}$ in EF from Fenton's reaction (2) improved DOC abatement up to a final mineralization of 86%, 90% and 91% for the above j values, as shown in Fig. 4b. In contrast, Fig. 4c reveals a slightly higher mineralization rate with raising j using PEF, being only noticeable until 120–180 min, when 82–86% mineralization was attained, whereupon a similar DOC decay occurred up to attaining 90%, 92% and 94% of mineralization at 360 min of 33.3, 66.7 and 100 mA cm^{-2} , respectively. This behavior suggests that UVA irradiation photolyzes so rapidly the photoactive intermediates while they are formed that the production of more hydroxyl

radicals at higher j did not improve significantly the mineralization rate of the RY160 solutions.

Fig. 5a–c presents the MCE values calculated from Eq. (10) for the experiments given in Fig. 4a–c, respectively. While higher j accelerated all the mineralization processes due to the generation of more oxidizing species and/or an effective photolysis of photoactive intermediates, the opposite trend can be observed for current efficiency since it gradually dropped. This phenomenon can be associated with the progressive increase in rate of non-oxidizing reactions of hydroxyl radicals, thereby promoting a smaller number of reactive events with organic molecules. Consequently, a clear decrease in current efficiency was observed. Examples of such parasitic reactions are the oxidation of BDD($\cdot\text{OH}$) to O_2 at the BDD anode by reaction (14) and the consumption of $\cdot\text{OH}$ in the bulk in the presence of H_2O_2 and Fe^{2+} through reactions (15) and (16), respectively [12,33]. The quicker generation of weaker oxidants at the anode such as $\text{S}_2\text{O}_8^{2-}$ from SO_4^{2-} of the electrolyte by reaction (17) and O_3 by reaction (18) plays also their role, both of them decreasing BDD($\cdot\text{OH}$) concentration that is available to oxidize organics [34].

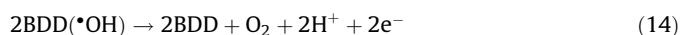


Fig. 5a–c also shows a decay of all MCE values with prolonging electrolyses owing to the gradual loss of organic load and the formation of more recalcitrant products [33]. Low current efficiencies (< 10%) were obtained in AO- H_2O_2 treatments, which dropped very slowly attaining final values from 5.6% to 2.5% by varying j between 33.3 and 100 mA cm^{-2} (see Fig. 5a). Much greater MCE values were found in the EF process at times < 180 min, but they further decayed very rapidly up to 8.1%, 3.7% and 2.9% for 33.3, 66.7 and 100 mA cm^{-2} , respectively (see Fig. 5b). Although the current efficiencies for PEF were clearly superior to those of EF until 120 min, they decayed so quickly at longer time in the former process that only slightly greater MCE values compared with the latter one were finally obtained (see Fig. 5c). These findings suggest a conversion of organics into CO_2 at similar rate by BDD($\cdot\text{OH}$) in the AO- H_2O_2 runs. In contrast, the higher MCE values in EF at short times are indicative of a much quicker destruction of organics by $\cdot\text{OH}$, which is enhanced in PEF by the synergistic action of UVA light on photoactive products.

The change of EC_{DOC} determined from Eq. (11) with the percentage of DOC removal for the above trials is depicted in Fig. 6a–c. As expected, the specific energy consumption increased when j was raised and diminished as the relative oxidation power of processes was enhanced. The lowest EC_{DOC} values were then obtained at $j = 33.3 \text{ mA cm}^{-2}$, being 1.73, 1.21 and 1.11 kWh g^{-1} DOC at the end of the AO- H_2O_2 , EF and PEF runs, respectively, all of them representing a volumetric consumption of about 52 kWh m^{-3} . This value is similar to that obtained for the treatment of other azo dyes under analogous conditions [39,40]. It is also noticeable from Fig. 6c that at high DOC removal of PEF treatments (77–79%), 0.44 kWh g^{-1} DOC were consumed at 33.3 mA cm^{-2} , being much lower than $1.3\text{--}1.4 \text{ kWh g}^{-1}$ DOC at 66.7 and 100 mA cm^{-2} . These

values corresponded to 17, 48 and 52 kWh m⁻³, respectively. This means that decreasing j allows obtaining similar mineralization up to about 80% DOC removal, but with much lower energy consumption, therefore being advantageous the use of low j (e.g., 33.3 mA cm⁻²) in terms of cost for the application of EAOPs to the remediation of wastewater containing RY160 azo dye.

3.4. Influence of azo dye concentration on the degradation processes

The study of the degradation of acidic RY160 solutions was extended to a greater concentration of 0.334 mmol dm⁻³ of the azo dye to check the effect of the initial organic load on the performance of all the EAOPs. Fig. 7 exemplifies the results obtained for $j = 100$ mA cm⁻² during 360 min of electrolysis. As can be seen in Fig. 7a, the loss of the solution color was accelerated in the sequence AO-H₂O₂ < EF < PEF, in agreement with the larger production of hydroxyl radicals, as pointed out above. A decolorization efficiency of 96% was attained at the end of AO-H₂O₂, whereas the solution became colorless after more than 300 min in EF and after 120 min in PEF, which were much longer times than those found for the less concentrated solution with 0.167 mmol dm⁻³ RY160, as shown in Fig. 2a. The decolorization rate then decreases at higher azo dye content, which can be simply associated with the slower destruction of more organic load by similar quantities of hydroxyl radicals originated at the same j value. A similar conclusion can be deduced by comparing the DOC abatements of Fig. 2b and 7b, since lower percentage of DOC removal at a given time was found upon AO-H₂O₂ and EF treatment of the 0.334 mmol dm⁻³ azo dye solution. For example, after 360 min of electrolysis, 75% and 82% of mineralization was obtained for these EAOPs with the latter solution, respectively (see Fig. 7b), whereas 79% and 81% of DOC abatement were found for the less concentrated solution (see Fig. 2b). In contrast, similar DOC reductions of 96% and 94% were determined at the end of PEF. This points to consider a very positive action of UVA irradiation regarding the mineralization of organics in this powerful procedure, which is maintained and even improved in the presence of greater amounts of pollutants.

The significant mineralization rate showed for the 0.334 mmol dm⁻³ azo dye solution by all the EAOPs was also reflected in higher MCE values (see Fig. 8a) and lower EC_{DOC} values (see Fig. 8b) compared to those of the less concentrated solution (see Fig. 5 and 6). At the end of the treatment, current efficiencies of 4.7%, 5.1% and 6.0% were obtained for AO-H₂O₂, EF and PEF, respectively, whereas the corresponding specific energy consumptions were of 4.7, 3.8 and 3.2 kWh g⁻¹ DOC. These results indicate that the EAOPs, and especially the powerful PEF, are more efficient and require a lower electrical consumption as azo dye content increases, suggesting that organics are more quickly removed by larger amounts of hydroxyl radicals available due to the deceleration of their parasitic reactions (14)–(18). This is advantageous for the application of these procedures to real wastewater treatment, since they usually contain high dye loads, usually between 100 and 250 mg dm⁻³ [38]. The alternative use of solar PEF could drastically reduce the excessive energy requirements of artificial UVA light utilized in PEF [26].

3.5. Identification of short-linear aliphatic carboxylic acids and released inorganic ions

The 0.167 mmol dm⁻³ RY160 solutions were analyzed at regular times by ion-exclusion HPLC during their electrolysis at 33.3 mA cm⁻² by the different EAOPs for 360 min to identify and quantify the final short-linear aliphatic carboxylic acids

produced. These chromatograms displayed well-defined peaks related to maleic, fumaric, tartronic, acetic, oxalic, oxamic and formic acids. The former four acids can proceed from the cleavage of the benzene rings of the azo dye (see Fig. 1), and they are subsequently oxidized to oxalic and formic acids [11,12,38–42]. In contrast, oxamic acid can be formed from the degradation of *N*-derivatives. Oxalic, oxamic and formic acids are final products that can be directly mineralized to CO₂ [9,12,42]. Note that all the acids form Fe(III)-carboxylate complexes to a large extent in the EF and PEF treatments [38–42]. The evolution of the most significant acids is illustrated in Fig. 9a–c for AO-H₂O₂, EF and PEF, respectively.

Maleic, fumaric and acetic acids were always accumulated in very low concentrations (<0.1 mg dm⁻³), disappearing from the medium within short times (<300 min) in all cases. Tartronic acid was only detected in EF and PEF, with maximum contents

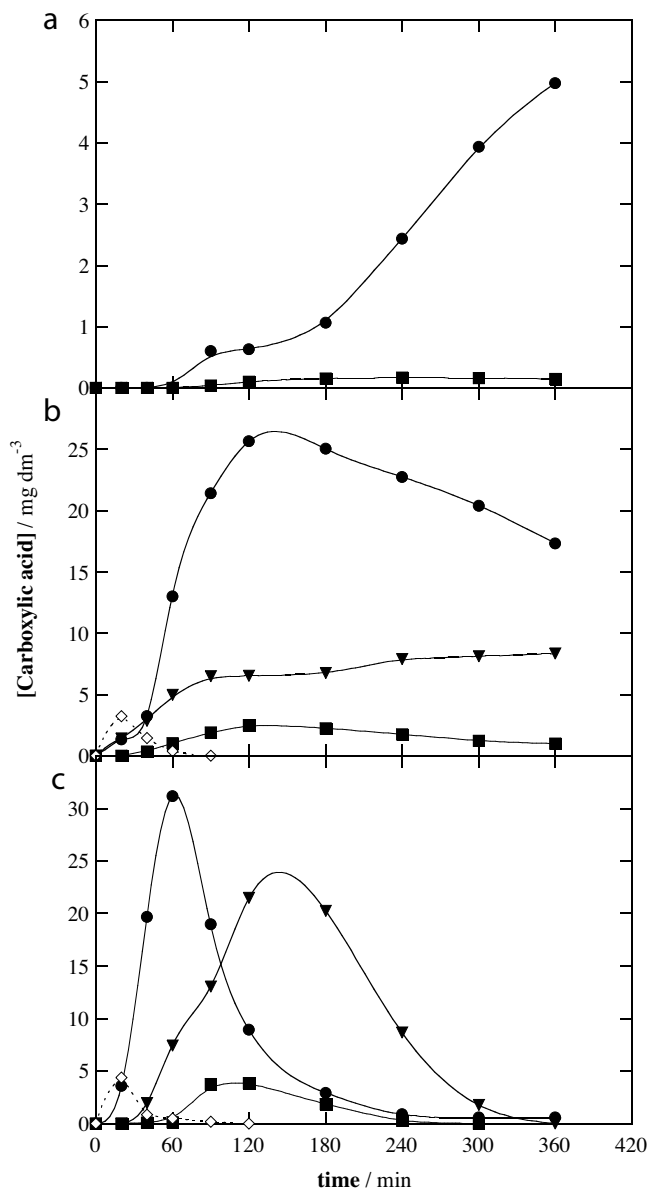


Fig. 9. Time-course of the concentration of (\diamond) tartronic, (\bullet) oxalic, (\blacksquare) oxamic and (\blacktriangledown) formic acids detected during the (a) AO-H₂O₂, (b) EF and (c) PEF degradation of 100 cm³ of a solution of 0.167 mmol dm⁻³ RY160 in 0.050 mol dm⁻³ Na₂SO₄ at pH 3.0 using a stirred BDD/air-diffusion tank reactor at 33.3 mA cm⁻² and 25 °C.

< 4.4 mg dm⁻³ at 20 min and total removal in about 90–120 min (see Fig. 9b and c). These findings are indicative of a quick removal of Fe(III)-maleate, Fe(III)-fumarate, Fe(III)-acetate and Fe(III)-tartronate complexes by hydroxyl radicals, mainly by BDD(*OH) [9,11]. A different behavior can be observed in Fig. 9a–c for the shorter carboxylic acids that were usually accumulated to a larger extent and for longer time. Oxamic acid only appeared with 0.17, 2.5 and 3.8 mg dm⁻³ as maximal in AO-H₂O₂, EF and PEF, respectively, reaching final contents of 0.15, 1.0 and 0.10 mg dm⁻³. The more pronounced accumulation of oxamic acid and the faster destruction of Fe(III)-oxamate complexes in PEF can be ascribed to the action of UVA light to produce higher amounts of oxidant *OH induced by reaction (5), to photo-oxidize *N*-derivatives and/or to destroy the Fe(III)-oxamate species via reaction (6). In turn, formic acid was not detected in AO-H₂O₂, but it was largely and continuously accumulated up to 8.3 mg dm⁻³ in EF (see Fig. 9b), suggesting that it was pre-eminently formed when intermediates were oxidized by *OH in the bulk, whereas Fe(III)-formate complexes were hardly destroyed by BDD(*OH) and *OH. In PEF, however, formic acid was totally removed at 360 min after achieving a maximal concentration of 21 mg dm⁻³ at 120 min. This means that UVA light contributed to the production of more formic acid, probably by the generation of more *OH, and photodecomposed very quickly the resulting Fe(III)-formate complexes up to their total disappearance. The same trend can be deduced from Fig. 9a–c for oxalic acid. It was progressively accumulated up to 5.0 mg dm⁻³ in AO-H₂O₂, because of its slow reaction with BDD(*OH), much largely accumulated up to 26 mg dm⁻³ with further slow decay to 17 mg dm⁻³ in EF, due to the slow oxidation of Fe(III)-oxalate species by hydroxyl radicals, and almost completely removed at the end of PEF, as a result of the effective photolysis of these complexes by UVA irradiation through reaction (6). A mass balance at the end of the treatments revealed that the remaining solutions in AO-H₂O₂, EF and PEF contained 1.4, 6.9 and 0.2 mg dm⁻³ of DOC related to all detected acids, respectively, which represented a 7.0%, 100% and 4.2% of their corresponding DOC (see Fig. 4). These findings allow inferring that the AO-H₂O₂ process led to large amounts of undetected products, even more recalcitrant than short-linear carboxylic acids to the attack by BDD(*OH), whereas the final solution of EF was composed pre-eminently by carboxylic acids thanks to the most effective oxidation of *OH in the bulk. In contrast, small quantities of highly recalcitrant products remained at the end of PEF, suggesting that they are the result of the photolytic action of UVA light on several intermediates.

Inorganic ions formed during the mineralization of the 0.167 mmol dm⁻³ RY160 solution in 0.050 mol dm⁻³ LiClO₄ as background electrolyte (to avoid the sulfate medium), regulated at pH 3.0 with HClO₄, at 33.3 mA cm⁻² were determined at the end of all the EAOPs by ion chromatography. In all cases, 3.3–3.4 mg dm⁻³ Cl⁻ ion, which is about 56% of the initial Cl content (5.92 mg dm⁻³), and 16.0 mg dm⁻³ SO₄²⁻ ion, accounting for 100% of the initial S concentration, were found. Since Cl⁻ can be oxidized to Cl₂ on the BDD anode [11,33], one can conclude that all the Cl and S atoms of the azo dye were completely released as Cl⁻ and SO₄²⁻ ions, as stated in the theoretical total mineralization reaction (9). On the other hand, its 9N atoms (21.04 mg dm⁻³) were pre-eminently transformed into NH₄⁺ ion and, to a smaller extent, into NO₃⁻ ion, as considered in reaction (9). The corresponding percentages of N determined for these ions were 18.7% and 6.4% in AO-H₂O₂, 20.3% and 7.0% in EF and 16.4% and 3.8% in PEF. Therefore, about 73–80% of the initial N was not accumulated in the form of these two anions and, in view of the high DOC removal attained in EF and PEF, it was probably lost as volatile N₂ or N_xO_y species, as also proposed for the mineralization processes of other azo dyes [38–42].

4. Conclusions

A 0.167 mmol dm⁻³ RY160 solution of pH 3.0 was slowly decolorized by AO-H₂O₂ using a BDD/air-diffusion tank reactor at 100 mA cm⁻² due to the slow destruction of the azo dye and its colored products by BDD(*OH). In contrast, a rapid decolorization was observed in EF with 0.50 mmol dm⁻³ Fe²⁺ because of the quicker attack of *OH formed in the bulk. The solution became colorless even more rapidly using PEF owing to the production of larger amounts of *OH induced by the photolysis of Fe(III)-hydroxy species. From DOC removal, it was established an increasing relative oxidation power of the EAOPs in the order AO-H₂O₂ < EF < PEF, in agreement with their decolorization trend. PEF was the most powerful EAOP, since the synergistic action of BDD(*OH), *OH and UVA light yielded 94% mineralization after 360 min. Higher *j* always accelerated the decolorization and mineralization, but it was detrimental regarding the current efficiency and the specific energy consumption. The treatment of more concentrated solutions was feasible by PEF, reaching 96% of mineralization after 360 min at 100 mA cm⁻². Oxalic, oxamic and formic acids were largely produced as final short-linear carboxylic acids. A large amount of other persistent products was accumulated in AO-H₂O₂, whereas a smaller number of highly recalcitrant products originated by UVA light was accumulated in PEF, thereby preventing the total mineralization. Chloride, sulfate, ammonium and nitrate were formed as inorganic ions from the heteroatoms of the azo dye. Our results prove the viability of PEF to treat wastewater containing azo dyes like RY160.

Acknowledgments

Financial support from MINECO (Spain) under the project CTQ2013-48897-C2-1-R, co-financed with FEDER funds, as well as from PRODEP-UGTO-PTC-472 and UGTO, Convocatoria Institucional para Fortalecer la Excelencia Académica 2015 (Mexico), is acknowledged.

References

- [1] E. Isarain-Chávez, C. de la Rosa, L.A. Godínez, E. Brillas, J.M. Peralta-Hernández, Comparative study of electrochemical water treatment processes for a tannery wastewater effluent, *J. Electroanal. Chem.* 713 (2014) 62.
- [2] R. Sanghi, B. Bhattacharya, Adsorption-coagulation for the decolorisation of textile dye solutions, *Water Qual. Res. J. Can.* 38 (2003) 553.
- [3] A.B. dos Santos, F.J. Cervantes, J.B. van Lier, Review paper on current technologies for decolourisation of textile wastewaters: perspectives for anaerobic biotechnology, *Bioresour. Technol.* 98 (2007) 2369.
- [4] A.K. Verma, R.R. Dash, P. Bhunia, A review on chemical coagulation/flocculation technologies for removal of colour from textile wastewaters, *J. Environ. Manage.* 93 (2012) 154.
- [5] T. Robinson, G. McMullan, R. Marchant, P. Nigam, Remediation of dyes in textile effluent: A critical review on current treatment technologies with a proposed alternative, *Biores. Technol.* 77 (2001) 247.
- [6] H. Zollinger, *Color Chemistry: Synthesis, Properties, and Applications of Organic Dyes and Pigments*, VCH and Wiley-VCH Switzerland (2003).
- [7] E. Forgacs, T. Cserhádi, G. Oros, Removal of synthetic dyes from wastewaters: A review, *Environ. Int.* 30 (2004) 953.
- [8] S. Pokharna, R. Shrivastava, Photocatalytic treatment of textile industry effluent using titanium oxide, *Int. J. Recent Res. Rev.* VI (2013) 9.
- [9] E. Brillas, I. Sirés, M.A. Oturan, Electro-Fenton process and related electrochemical technologies based on Fenton's reaction chemistry, *Chem. Rev.* 109 (2009) 6570.
- [10] S. Vasudevan, M.A. Oturan, Electrochemistry: as cause and cure in water pollution—an overview, *Environ. Chem. Lett.* 12 (2014) 97.
- [11] I. Sirés, E. Brillas, M.A. Oturan, M.A. Rodrigo, M. Panizza, Electrochemical advanced oxidation processes: today and tomorrow. A review, *Environ. Sci. Pollut. Res.* 21 (2014) 8336.
- [12] E. Brillas, C.A. Martínez-Huitle, Decontamination of wastewaters containing synthetic organic dyes by electrochemical methods. An updated review, *Appl. Catal. B: Environ.* 166–167 (2015) 603.
- [13] A. Khataee, A. Khataee, M. Fathinia, B. Vahid, S.W. Joo, Kinetic modeling of photoassisted-electrochemical process for degradation of an azo dye using boron-doped diamond anode and cathode with carbon nanotubes, *J. Ind. Eng. Chem.* 19 (2013) 1890.

- [14] A. Khataee, A. Akbarpour, B. Vahi, Photoassisted electrochemical degradation of an azo dye using Ti/RuO₂ anode and carbon nanotubes containing gas-diffusion cathode, *J. Taiwan Inst. Chem. Eng.* 45 (2014) 930.
- [15] A. Wang, J. Qu, H. Liu, J. Ru, Mineralization of an azo dye Acid Red 14 by photoelectro-Fenton process using an activated carbon fiber cathode, *Appl. Catal. B: Environ.* 84 (2008) 393.
- [16] I. Yamanka, T. Hashimoto, R. Ichihashi, K. Otsuka, Direct synthesis of H₂O₂ acid solutions on carbon cathode prepared from activated carbon and vapor-growth-carbon-fiber by a H₂/O₂ fuel cell, *Electrochim. Acta* 53 (2008) 4824.
- [17] N. Daneshvar, S. Aber, V. Vatanpour, M.H. Rasoulifard, Electro-Fenton treatment of dye solution containing Orange II: Influence of operational parameters, *J. Electroanal. Chem.* 615 (2008) 165.
- [18] M. Rivera, M. Pazos, M.A. Sanromán, Development of an electrochemical cell for the removal of Reactive Black 5, *Desalination* 274 (2011) 39.
- [19] M. Panizza, M.A. Oturan, Degradation of Alizarin Red by electro-Fenton process using a graphite-felt cathode, *Electrochim. Acta* 56 (2011) 7084.
- [20] N. Oturan, E. Brillas, M.A. Oturan, Unprecedented total mineralization of atrazine and cyanuric acid by anodic oxidation and electro-Fenton with a boron-doped diamond anode, *Environ. Chem. Lett.* 10 (2012) 165.
- [21] M.S. Yahya, N. Oturan, K. El Kacemi, M. El Karbane, C.T. Aravindakumar, M.A. Oturan, Oxidative degradation study on antimicrobial agent ciprofloxacin by electro-Fenton process: Kinetics and oxidation products, *Chemosphere* 117 (2014) 447.
- [22] A. El-Ghenmy, R.M. Rodríguez, E. Brillas, N. Oturan, M.A. Oturan, Electro-Fenton degradation of the antibiotic sulfanilamide with Pt/carbon-felt and BDD/carbon-felt cells. Kinetics, reaction intermediates, and toxicity assessment, *Environ. Sci. Pollut. Res.* 21 (2014) 8368.
- [23] F. Sopaj, M.A. Rodrigo, N. Oturan, F.I. Podvorica, J. Pinson, M.A. Oturan, Influence of the anode materials on the electrochemical oxidation efficiency. Application to oxidative degradation of the pharmaceutical amoxicillin, *Chem. Eng. J.* 262 (2015) 286.
- [24] B. Boye, M.M. Dieng, E. Brillas, Electrochemical degradation of 2,4,5-trichlorophenoxyacetic acid in aqueous medium by peroxi-coagulation. Effect of pH and UV light, *Electrochim. Acta* 48 (2003) 781.
- [25] S. Garcia-Segura, J.A. Garrido, R.M. Rodríguez, P.L. Cabot, F. Centellas, C. Arias, E. Brillas, Mineralization of flumequine in acidic medium by electro-Fenton and photoelectro-Fenton processes, *Water Res.* 46 (2012) 2067.
- [26] S. Garcia-Segura, E. Brillas, Advances in solar photoelectro-Fenton: Decolorization and mineralization of the Direct Yellow 4 diazo dye using an autonomous solar pre-pilot plant, *Electrochim. Acta* 140 (2014) 384.
- [27] A. Thiam, E. Brillas, F. Centellas, P.L. Cabot, I. Sirés, Electrochemical reactivity of Ponceau 4R (food additive E124) in different electrolytes and batch cells, *Electrochim. Acta* 173 (2015) 523.
- [28] K. Cruz-González, O. Torres-López, A. García-León, J.L. Guzmán-Mar, L.H. Reyes, A. Hernández-Ramírez, J.M. Peralta-Hernández, Determination of optimum operating parameters for Acid Yellow 36 decolorization by electro-Fenton process using BDD cathode, *Chem. Eng. J.* 160 (2010) 199.
- [29] K. Cruz-González, O. Torres-López, A.M. García-León, E. Brillas, A. Hernández-Ramírez, J.M. Peralta-Hernández, Optimization of electro-Fenton/BDD process for decolorization of a model azo dye wastewater by means of response surface methodology, *Desalination* 286 (2012) 63.
- [30] A. Uranga-Flores, C. de la Rosa-Júarez, S. Gutierrez-Granados, D. Chianca de Moura, C.A. Martínez-Huitle, J.M. Peralta-Hernandez, Electrochemical promotion of strong oxidants to degrade Acid Red 211: Effect of supporting electrolytes, *J. Electroanal. Chem.* 738 (2015) 84.
- [31] J.M. Peralta-Hernández, L.A. Godínez, Electrochemical hydrogen peroxide production in acidic medium using a tubular photo-reactor: Application in advanced oxidation processes, *J. Mex. Chem. Soc.* 58 (2014) 348.
- [32] C.A. Martínez-Huitle, M.A. Rodrigo, I. Sirés, O. Scialdone, Single and coupled electrochemical processes and reactors for the abatement of organic water pollutants: A critical review, *Chem. Rev.* 115 (2015) 13362.
- [33] M. Panizza, G. Cerisola, Direct and mediated anodic oxidation of organic pollutants, *Chem. Rev.* 109 (2009) 6541.
- [34] E. Guinea, E. Brillas, F. Centellas, P. Cañizares, M.A. Rodrigo, C. Sáez, Oxidation of enrofloxacin with conductive-diamond electrochemical oxidation, ozonation and Fenton oxidation. A comparison, *Water Res.* 43 (2009) 2131.
- [35] E. Tsantaki, T. Velegraki, A. Katsaounis, D. Mantzavinos, Anodic oxidation of textile dyehouse effluents on boron-doped diamond electrode, *J. Hazard. Mater.* 207–208 (2012) 91.
- [36] M.A. Quiroz, J.L. Sánchez-Salas, S. Reyna, E.R. Bandala, J.M. Peralta-Hernández, C.A. Martínez-Huitle, Degradation of 1-hydroxy-2,4-dinitrobenzene from aqueous solutions by electrochemical oxidation: role of anodic material, *J. Hazard. Mater.* 268 (2014) 6.
- [37] M.J. Martín de Vidales, S. Barba, C. Sáez, P. Cañizares, M.A. Rodrigo, Coupling ultraviolet light and ultrasound irradiation with conductive-diamond electrochemical oxidation for the removal of progesterone, *Electrochim. Acta* 140 (2014) 20.
- [38] E.J. Ruiz, A. Hernández-Ramírez, J.M. Peralta-Hernández, C. Arias, E. Brillas, Application of solar photoelectro-Fenton technology to azo dyes mineralization: Effect of current density, Fe²⁺ and dye concentration, *Chem. Eng. J.* 171 (2011) 385.
- [39] F.C. Moreira, S. Garcia-Segura, V.J.P. Vilar, R.A.R. Boaventura, E. Brillas, Decolorization and mineralization of Sunset Yellow FCF azo dye by anodic oxidation, electro-Fenton, UVA photoelectro-Fenton and solar photoelectro-Fenton processes, *Appl. Catal. B: Environ.* 142–143 (2013) 877.
- [40] X. Florenza, A.M.S. Solano, F. Centellas, C.A. Martínez-Huitle, E. Brillas, S. Garcia-Segura, Degradation of the azo dye Acid Red 1 by anodic oxidation and indirect electrochemical processes based on Fenton's reaction chemistry. Relationship between decolorization, mineralization and products, *Electrochim. Acta* 142 (2014) 276.
- [41] A. Thiam, I. Sirés, J.A. Garrido, R.M. Rodríguez, E. Brillas, Effect of anions on electrochemical degradation of azo dye Carmoisine (Acid Red 14) using a BDD anode and air-diffusion cathode, *Sep. Purif. Technol.* 140 (2015) 43.
- [42] A. Thiam, I. Sirés, E. Brillas, Treatment of a mixture of food color additives (E122 E124 and E129) in different water matrices by UVA and solar photoelectro-Fenton, *Water Res.* 81 (2015) 178.
- [43] Y. Zuo, J. Hoigné, Formation of hydrogen peroxide and depletion of oxalic acid in atmospheric water by photolysis of iron(III)-oxalato complexes, *Environ. Sci. Technol.* 26 (1992) 1014.
- [44] M. Gaber, N.A. Ghalwa, A.M. Khedr, M.F. Salem, Electrochemical degradation of Reactive Yellow 160 dye in real wastewater using C/PbO₂-, Pb+Sn/PbO₂+SnO₂-, and Pb/PbO₂ modified electrodes, *J. Chem.* 2013 (2013) Article ID 691763, 9 pages.
- [45] S. Garcia-Segura, F. Centellas, C. Arias, J.A. Garrido, R.M. Rodríguez, P.L. Cabot, E. Brillas, Comparative decolorization of monoazo, diazo and triazo dyes by electro-Fenton process, *Electrochim. Acta* 58 (2011) 303.
- [46] F.J. Welcher (Ed.), *Standard Methods of Chemical Analysis*, Vol. 2, Part B, 6th ed., R.E. Krieger Publishers, Huntington, New York, 1975, p. 1827.